HORIZON 2020

Research Infrastructures

H2020-INFRAIA-2014-2015

INFRAIA-1-2014-2015 Integrating and opening existing national and regional research infrastructures of European interest

ENSAR2

European Nuclear Science and Application Research 2

Grant Agreement Number: 654002

D13.2 - Code ENSARRoot with generic codes with specific reactions and tracking

Version: 2.0
Author: N Kalantar
Date: 27/02/2020

PROJECT AND DELIVERABLE INFORMATION SHEET

ENSAR2 Project Ref. №	654002
Project Title	European Nuclear Science and Application Research 2
Project Web Site	http://www.ensarfp7.eu/
Deliverable ID	D13.2
Deliverable Nature	Other
Deliverable Level*	PU
Contractual Date of Delivery	29/02/2020
Actual Date of Delivery	27/02/2020
EC Project Officer	René Martin

* The dissemination level are indicated as follows: PU – Public, PP – Restricted to other participants (including the Commission Services), RE – Restricted to a group specified by the consortium (including the Commission Services). CO – Confidential, only for members of the consortium (including the Commission Services).

DOCUMENT CONTROL SHEET

Document	Title: Code ENSARRoot with generic codes with specific reactions and tracking	
	ID:D13.2	
	Version: 0.1	
	Available at: http://www.ensarfp7.eu/	
	Software Tool: Microsoft Office Word 2007	
	File:	
Authorship	Written by:	N. Kalantar
	Contributors:	
	Reviewed by:	Y. Leifels, GSI
	Approved by:	M.N. Harakeh, KVI CART

DOCUMENT STATUS SHEET

Version	Date	Status	Comments
0.1	25/02/2020	For internal review	
1.0	27/02/2020	For internal review	
2.0	27/02/2020	Submitted on EC Participant Portal	
		Final version	

DOCUMENT KEYWORDS

Keywords	Code ENSARRoot, Tracking algorithms, CALIFA

Disclaimer

This deliverable has been prepared by Work Package 13 (Simulations and Analysis Tools for Nuclear Reactions and Structure in Europe) of the Project in accordance with the Consortium Agreement and the Grant Agreement n°654002. It solely reflects the opinion of the parties to such agreements on a collective basis in the context of the Project and to the extent foreseen in such agreements.

Copyright notices

TABLE OF CONTENTS

LIST OF FIGURES

REFERENCES AND APPLICABLE DOCUMENTS
[1]

LIST OF ACRONYMS AND ABBREVIATIONS

EXECUTIVE SUMMARY

This deliverable reports on the results related to **Task 2 "Development of analysis tools"** of the SATNuRSE (Simulations and Analysis Tools for Nuclear Reactions and Structure in Europe) Work Package of the ENSAR2 IntegratingAactivity.

INTRODUCTION

The ENSARRoot framework was developed during the working period of the previous ENSAR project as a platform for the simulation and analysis of nuclear-physics experimental setups. The code has been improved during the last years implementing new tracking algorithms and new applications, which will be described in the present report. Additionally, there has been a notable effort in the development of a novel track-reconstruction and pattern recognition algorithm based on Artificial Neural Networks that it is also reported here.

General information on ENSARRoot is presented in the first section, detailing the status and availability of the code. The second section in this report corresponds to the implementation of the time tracking algorithm TimTrack in ENSARRoot and the related applications. Next, the CALIFA Gamma Benchmark Experiment to characterise the crystal response of the CALIFA (CALorimeter for In-Flight detection of gamma-rays and high-energy charged pArticles) detector for future experiments at FAIR/GSI (Germany) and PIGE experiment implementations are described. Finally, in the last section, a description of the development of a Deep Neural Network (DNN) for the data analysis of the NeuLAND neutron detector is given.

SECTION 1 GENERAL ENSARROOT INFORMATION

ENSARRoot is a framework for simulation and data analysis for the ENSAR/SiNuRSE and ENSAR2/SATNuRSE activities, based on the FAIRRoot framework [1].

FAIRRoot is a simulation, reconstruction and analysis framework that is based on the ROOT system. GEANT3 and GEANT4 transport engines are supported in a clever way: the user code that creates simulated data does not depend on a particular Monte-Carlo engine. The framework offers base classes, which enable users (or other derived packages) to construct their detectors and/or analysis tasks. It also has some general functionality like track visualisation.

ENSARRoot is available in the GitHub repository [2]. A description of the code and some of the applications included are also available [3].

SECTION 2 TRACKING ALGORITHMS IMPLEMENTATIONS

The TimTrack algorithm [4] for particle track reconstruction has been implemented in the code ENSARRoot as a common tracking service. In the present implementation, it was included in the class TraRPCHit2Saeta of the TRAGALDABAS module of ENSARRoot, which can be called from any task in the code.

Although TimTrack is a multi-plane algorithm, for practical purposes, only cases up to four detection planes have been implemented so far.

Using the present implementation of TimTrack, two important applications were developed within ENSARRoot:

- Muon Tomography in MuTT: MuTT is a commercial muon tomography system intended for the detection of heavy materials inside ship containers [5]. The geometry and performance of the system was implemented in ENSARRoot. In addition, the tomography imaging reconstruction procedure based on the TimTrack algorithm was developed.

- Particle Identification in TRAGALDABAS: TRAGALDABAS [6] is a cosmic ray telescope dedicated to the measurements of extensive air showers and their relation with the properties of the atmosphere. The detection system, as well as a complete description of the building where it is located, have been fully implemented in ENSARRoot. In addition, a particle identification tool for cosmic rays, based on TimTrack, called MIDAS [7], was developed and implemented in the framework as well.

An interface for the CRY Cosmic Ray Air Shower Library [8] was created and implemented in ENSARRoot. It corresponds to the class EnsarCryAsciiGenerator, located at the *ensargen* module, which allows for a direct use of the CRY ascii output into any ENSARRoot simulation.

Additionally, a multi-purpose Cosmic Ray Air Showers particle generator at the ground level was designed and implemented as a general event generator in ENSARRoot: Muons, electrons (and positrons) and photons are generated following the well-known energy and angular distributions of Cosmic Rays, and weighted by the well-known fluxes. This event generator allows for quicker simulations than those with "standard" Cosmic Ray event generators, since only the very last product of the shower is created.

This event generation is driven by the class EnsarTestGenerator, located at the *ensargen* module of ENSARRoot.

SECTION 3 IMPLEMENTATION OF BENCHMARKS AND EXPERIMENTAL SETUPS

Descriptions of two experiments at CTN/IST (Lisbon) are included in ENSARRoot: a CALIFA gamma benchmark experiment, whose goal was to characterise the crystal response of the CALIFA detector for future experiments at GSI/FAIR (Germany); and a PIGE (Particle-Induced Gamma-ray Emission) experiment, with the aim of expanding the available IBANDL data sets of some light isotopes. In order to complement the previous simulations, some analysis and particle generators have been developed, such as, gamma generators reproducing the correlated emission of photons emitted in nuclear cascades or radioactive chains to reproduce the environmental gamma background.

A: The CALIFA Gamma Benchmark Experiment

The purpose of this project is to simulate an experiment done at CTN/IST (Lisbon) in November 2016, studying $^{27}Al(p,\gamma)^{28}Si$ reaction at proton energies below 3 MeV. The experiment allows a precise identification of ^{28}Si excited states, giving us the possibility to study angular correlations in the decay of high-energy states and a characterisation of the response of the CsI(Tl) crystals of CALIFA with high-energy gamma rays. The CALIFA detector is one of the key detectors of the R^{3}B experiment at GSI (Germany), which surrounds the reaction chamber, acting as a calorimeter and a gamma-ray spectrometer.

The experimental setup consists of two sectors of CALIFA, each containing 64 crystals placed inside a trapezoidal aluminium box, and one HPGe (High Purity Germanium detector). The CALIFA detectors were placed at 90° and 180°, the HPGe at 270° with respect to the beam direction. Moreover, some inactive parts had been included as the

reaction chamber in order to obtain an accurate simulation. Figure 1 shows the setup design in the event viewer of the ENSARRoot simulation.
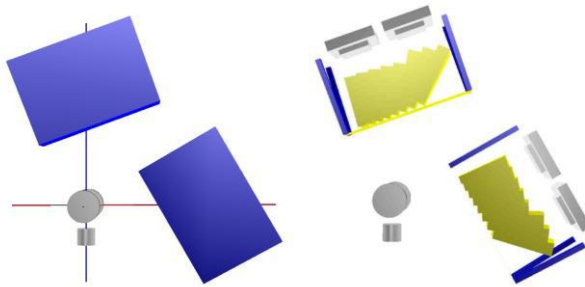

Fig. 1. View of the setup in the event viewer of the ENSARRoot simulation. On the left, on the z-x plane, there are two CALIFA sections (blue boxes), at the bottom a HPGe detector and, in the centre, the reaction chamber. On the right, the crystals inside each box are visible.

The gamma rays produced in the de-excitation of a certain nucleus are affected by the spectroscopic properties (i.e. its spin and parity) of the initial and final states. Therefore, they are emitted following a certain angular distribution. If they are emitted in a cascade, they show a characteristic angular correlation. In order to reproduce this effect in our simulation, we have developed a specific angular correlated gamma cascade generator. The three main components that we included are the energy of the gammas, the branching ratios and the expected angular correlation for each energy level. As these elements are the inputs of the generator, it is possible to use the same generator to reproduce diverse gamma cascade from any nucleus. A simple angular correlated gamma cascade from the excited states of ^{28}Si has been simulated in order to validate the ENSARRoot code developments (Fig. 2).
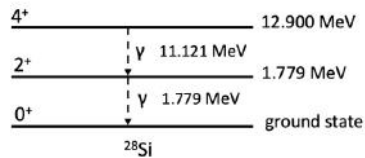

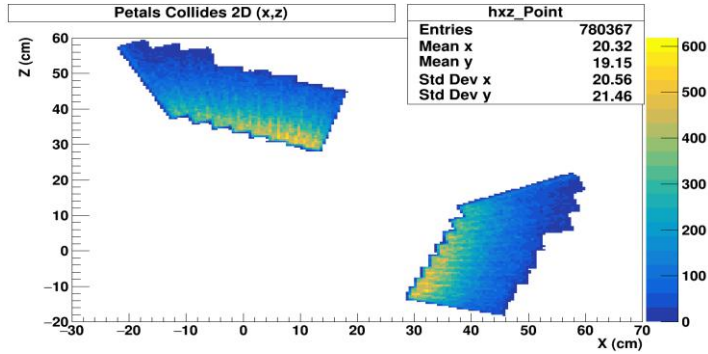*Fig. 2. A simple two-gamma cascade of the ^{28}Si de-excitation.*

Fig. 3. Number of photons arriving to each crystal of the CALIFA petals.

As we observe in Fig. 3, the angular coverage of each crystal depends on its position and on its intrinsic shape. Therefore, some corrections have been made using isotropic simulations to obtain the real angular dependence plotted in Fig. 4. In this figure, each dot represents one crystal signal and they fit with the theoretical angular correlation function (green line).
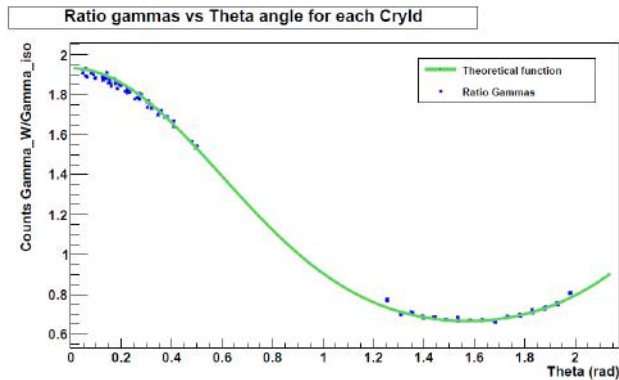
Fig. 4. Simulation of the gamma angular correlations using the developed Gamma Cascade Generator and the theoretical angular correlation function for a $4^+ \rightarrow 2^+ \rightarrow 0^+$ transition.

The analysis of environmental radiation is a challenging field, as it varies depending on altitude, the type of soil, etc.. All these variables and uncertainties make it difficult to predict the natural gamma background at a specific region beforehand. In this work, we focused on the simulation of the radioactive chains and the decay of ^{40}K, considering all the photon emissions from the nuclear decays which have a probability higher than 1% (in Fig. 5, all the contributions are plotted). One element that had to be included in the simulation of the setup is the soil effect because the energy loss of photons passing through the ground varies at different energies. This effect does not affect the potassium decay because it usually comes from the surroundings such as walls.
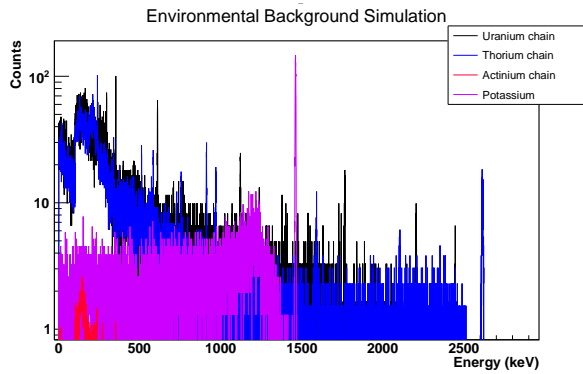
Fig. 5. Contribution of the radioactive chains and ⁴⁰K decay simulation in a HPGe detector.

Afterwards, summing and only applying a scale factor for each chain, which depends on the environmental characteristics of the laboratory, the natural radioactivity is simulated and compared to the real data, as we can observe in Fig. 6. The environmental data shown in this plot have been measured at CTN/IST laboratory in Lisbon (Portugal).

SECTION 4 TRACKING ALGORITHMS IMPLEMENTATIONS
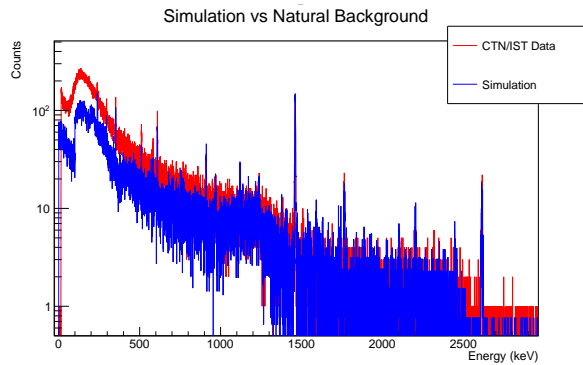
Fig. 6. Benchmarking between the background simulation and the environmental background measured at CTN/IST using HPGe detector.

There is a good agreement between the simulation and the measurements of environmental radiation. We observe some discrepancies, mostly at low energies, showing that the simulation of cosmic rays is needed. We are presently working on the inclusion of this component.

Experimental data have been measured in different locations of Portugal with different rates of natural radioactivity in order to check the flexibility of the code. Fig. 7 shows the data measurements at two locations in Portugal, at CTN/IST (Lisbon) and at Universidade de Beira Interior (Covilhã) where the radioactivity is higher. Therefore, one of the main assets of this background generator is that it could be used with any type of detector placed at different sites. Nowadays, we are putting special effort to reproduce the characteristic details of each environmental component in order to obtain an accurate and realistic background simulation for these distinct locations.
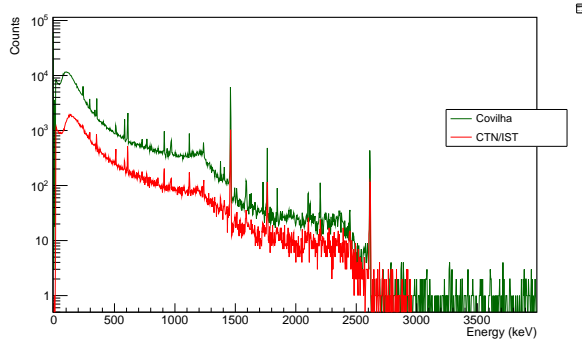

Fig. 7. Environmental radioactivity measured during 30 minutes using a HPGe detector with similar shape at CTN/IST, Lisbon (red line) and at Universidade da Beira Interior, Covilhã (green line).

B: PIGE Experiment and Analytical Tools

Taking the advantage that ENSARRoot allows the data treatment regardless of its origin, simulation or experiment, some analytical tools have been developed in order to explore PIGE (Particle-Induced Gamma-Ray Emission) technique and its limitations.

PIGE is one of the Ion Beam Analysis (IBA) group of analytical techniques that is widely used in applications ranging from environment to cultural heritage. Its multi-elemental analysis allows the determination of the concentration and an isotopical differentiation for light elements, i.e. $Z<20$. The PIGE technique uses proton, deuteron, or α- beams at low energies up to 4 MeV to surmount the repulsive Coulomb barrier where nuclear forces at low energy are involved. The basic mechanism is the formation of a compound nucleus in a highly excited state that de-excites by the emission of gamma rays. Therefore, it is restricted to the detection of gamma rays emitted in inelastic scattering and (p,γ) and (p,αγ) nuclear reactions.

Considering the lack of information on the chlorine stable isotopes, ^{35}Cl and ^{37}Cl, in the available IBANDL data set for PIGE analysis, our goal was to complete the cross section and yield data for these two isotopes at low energies using the versatility of ENSARRoot framework. The experimental campaign has taken place at the CTN/IST Laboratory (Sacavém) using a HPGe detector. The photons coming from the ^{35}Cl first- and the second-excited states are plotted depending on the proton beam energy in Figs. 8 and 9, respectively.
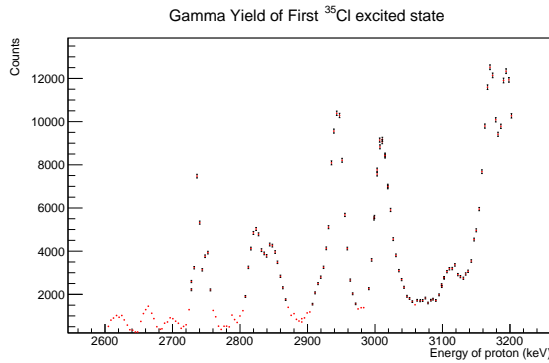
Gamma Yield of First ^{35}Cl excited state

Fig. 8. Experimental analysis of the ^{35}Cl first-excited state from the reaction ^{35}Cl(p,p'γ)^{35}Cl. (Preliminary Data)

Gamma Yield of Second ^{35}Cl excited state
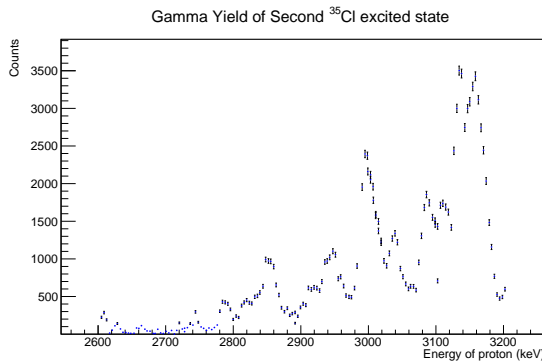
Fig. 9. Experimental analysis of the ^{35}Cl second-excited state from the reaction ^{35}Cl(p,p'γ)^{35}Cl. (Preliminary Data)

Apart from the experimental simulation that has been carried out, different methods and subroutines will be implemented in the code to treat the experimental data and the simulated data. As a result, an exhaustive benchmark between the experiment and the different parts of the simulation including the analytical methods will be performed.

SECTION 5 DEVELOPMENT OF A DEEP NEURAL NETWORK FOR THE DATA ANALYSIS OF THE NEuLAND NEUTRON

NeuLAND (Neu Large-Area Neutron Detector) [9] is the new neutron detector for the R^{3}B-experiment [10] in NUSTAR, FAIR [3]. NeuLAND [9] is meant to detect high-energy neutrons in the range 200 MeV – 1000 MeV [12] coming from nuclear reactions measured in inverse kinematics. One of its design goals is the detection of multiple neutrons within the same event.

NeuLAND has a modular design. In its final configuration, it will consist of 30 modules, called double-planes (dp). Each dp has an active area of 2.5 m by 2.5 m and a thickness of 10 cm. It consists of 50 square scintillators (5 cm thick and 2.5 m long each) in horizontal orientation, followed by another 50 such scintillators in vertical orientation. Neutrons can be detected due to their ability to undergo hadronic interactions with the scintillator material, which can produce charged particles.

The problem that we wish to address is the following: each neutron can give rise to any number of signals (fired scintillators) between one and a hundred. This leads to the problem of how to find the signal corresponding to the first interaction of the neutron with the detector [9], which is a prerequisite for reconstructing the neutrons 4-momentum vector. Since this first signal is the beginning of a particle shower in NeuLAND, we shall refer to this signal as the 'showerhead' from now on. The problem of finding the showerheads among all signals in NeuLAND is challenging, especially for events with multiple neutrons; several solutions have already been proposed in the literature [9,13].

The available methods in the literature for identifying the showerheads in NeuLAND have their shortcomings. The most important of these shortcomings is efficiency: how often one succeeds in correctly identifying the showerheads. Having a good efficiency for identifying the showerheads is important as this determines the beam time spent for an experiment. Today, there is still a large discrepancy between the efficiency NeuLAND can theoretically achieve and the actual efficiency of the known showerhead identification algorithms [13]. For this reason, we have developed a new showerhead identification algorithm using Deep Neural Networks (DNNs) [14, 15] to significantly improve the efficiency of the showerhead identification in NeuLAND.

A: Methodology

The use of DNNs in the NeuLAND data analysis is best explained through Fig. 10. This gives a comprehensive overview of the different steps that have to be taken for the showerhead identification in NeuLAND. The Signals (central in Fig. 10) are {E,t,x,y,z}-tuples (one for each fired scintillator) containing the relevant data of NeuLAND. One can either obtain them through the experiment or the Monte Carlo simulations and digitisation [16] of the setup used in the experiment. The clustering is done in the customary way for NeuLAND: two signals belong to the same cluster if $\Delta(x,y,z) < 7.5$ cm and $\Delta t < 1.0$ ns [9].
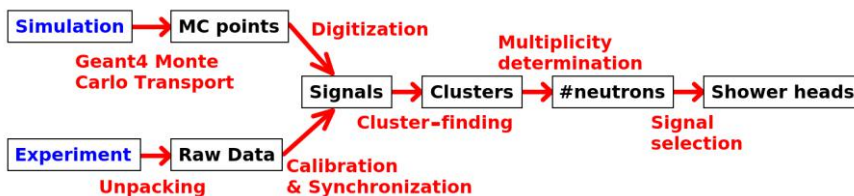
Fig. 10: The Different steps in the NeuLAND data analysis.

We have considered the use of DNNs for the last two steps in Fig. 10, namely the multiplicity determination and the signal selection. For the multiplicity determination, we have used the same DNN and training procedure as was used in [17], with a few minor improvements. This procedure was chosen because reference [17] was not only successful in improving the efficiency for multiplicity determination, but also contained a systematic search for the optimal DNN structure. For the signal selection, our method was inspired by the scoring method in [13]. However, instead of using histograms and cuts, we calculated the cluster score by the use of a DNN which used 14 different cluster properties

(like total energy, number of hits, length, Time-of-Flight, etc.) to extract the total cluster score. The DNN had similar properties to the multiplicity DNN. The source code of our method has been published as open source under license [18].

B: Some Results

The efficiency of the multiplicity determination is illustrated in Fig. 11 for events with 1 – 5 neutrons and a neutron energy of 600 MeV (and a relative energy of 500 keV, one of the standard NeuLAND simulation scenarios [13]). Computations were done for NeuLAND configurations of 8 dp, 16 dp and 30 dp. These configurations were chosen, because 8 dp are being used in the current R^{3}B experimental campaign, 16 dp currently have secured funding and the design goal for NeuLAND is 30 dp [9]. The red lines show the DNN performance. This is compared to the traditional method for multiplicity determination (blue lines), introduced in the NeuLAND Technical Design Report (TDR) [9,13,16]. The maximum possible performance is also indicated as a solid black line. This black line was computed by tracing the neutron showers in the Monte-Carlo simulation that produced the signals (see Fig. 10), and is therefore referred to as 'Perfect Tracking'.
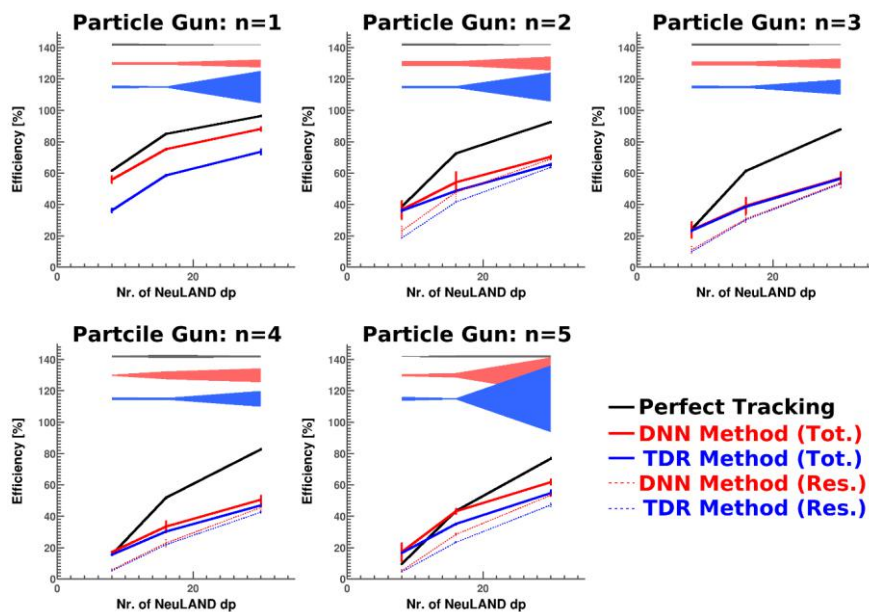
Fig. 11: Multiplicity performance of the DNN algorithm, the TDR algorithm and Perfect Tracking (maximum possible performance) for a neutron energy of 600 MeV. Results were computed for NeuLAND configurations of 8 dp, 16 dp and 30 dp. Connecting lines are drawn to guide the eye. See text for further details.

The solid red and blue lines show the DNN and TDR performance, as it would be measured during an experiment. As can be seen in Fig. 11, this performance sometimes goes above the perfect-tracking curve. This is because some events are 'accidentally' assigned to the correct multiplicity. To understand how this works, consider a 4-neutron

event where three neutrons interact with NeuLAND and the fourth penetrates NeuLAND without any interaction. In such an event, the multiplicity determination algorithm (either TDR or DNN) may mistake the interactions of the three neutrons for four. Hence, the correct particle gun multiplicity is assigned, even though the fourth neutron was not detected. Since the Perfect Tracking only identifies which neutrons are detected (by tracing their showers), 'accidentally' correct assignments cannot occur here. As a result, the solid red and blue lines can sometimes be larger than the solid black line. The red and blue dashed lines show the restricted (Res.) performance: the performance when these 'accidental' correct assignments are excluded (which can only be done for simulation data).

From Fig. 11, it is clear that the DNN performance is better than the conventional TDR performance, although differences are sometimes small (especially for 3 and 4 neutron events). However, the DNN result is consistently higher than the TDR result for all studied NeuLAND configurations (8 dp, 16 dp and 30 dp) and for both the full as well as the restricted performance (solid and dashed lines, respectively). Similar results were obtained for neutron energies of 200 MeV and 1000 MeV. Hence, we conclude that our DNN algorithm offers a (small) improvement in performance over the conventional method (TDR) as far as the multiplicity performance is concerned. However, since the fraction of 'accidentally correct' multiplicities is relatively large for 8 dp, we conclude that the number of NeuLAND dp should be larger than 8.

The separate error bands in Fig. 11 are estimates of the physics-list uncertainties. These uncertainties were estimated by varying the physics list between QGSP_INCLXX_HP and QGSP_BERT_HP for both training and validation. These two physics lists were benchmarked in [13] against experimental data for the single-neutron detection efficiency at 110 MeV and 250 MeV. It was found that reality was about halfway between these physics lists. The physics-list uncertainties in Fig. 11 offer an extra argument in favour of the DNN algorithm, as they are sometimes smaller than those for the TDR algorithm.

In order to study the performance of the signal selection procedure, it is necessary to consider the full 4-momenta of the neutrons involved [13]. Because of NeuLAND's design goal for multi-neutron detection and its use in the recent tetra-neutron experiment [19] we decided that the most illustrative method to demonstrate the performance of the signal selection procedure is to consider 4-neutron invariant mass spectra. Such spectra are shown in Fig. 12 for neutron energies of 600 MeV and NeuLAND configurations of 8 dp, 16 dp and 30 dp. Four times the free neutron mass was subtracted from the total invariant mass, which is why the x-axis is labelled 'Invariant Mass Difference'.
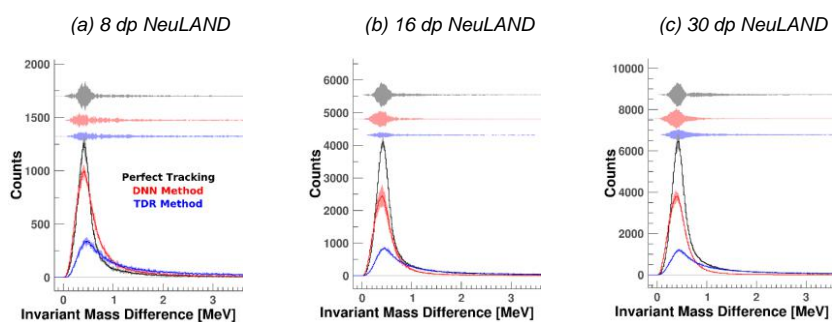

Fig. 12: Four-neutron invariant-mass spectra for 600 MeV neutrons and various NeuLAND configurations.

From Fig. 12, it follows that for 600 MeV neutrons, the DNN algorithm offers about a factor 3 higher efficiency than the previous TDR algorithm [9,13]. However, considering the relatively small improvements in Fig. 11, we must conclude that most of the gain in Fig. 12 comes from the improved signal selection method. Considering the relatively small physics-list uncertainties in Fig. 12 as well, it would seem that our new DNN algorithm offers a substantial improvement over the old algorithm.

Our simulations show that the situation for 1000 MeV neutrons is about the same as for Fig. 12 for the configurations of 16 dp and 30 dp. For the 8 dp configuration, the efficiency is also about a factor 3 larger, but the statistical uncertainties are much larger as well. For 200 MeV neutrons, the physics-list uncertainties are about a factor 3 larger for all three configurations (8 dp, 16 dp and 30 dp), while the increase in efficiency is only 50%.

As such, we conclude that the new DNN algorithm offers a substantial improvement in efficiency (statistics) for all neutron energies and configurations. However, in some of these situations (8 dp or 200 MeV) either the statistical or the physics-list uncertainties are too large to benefit from this improved efficiency. Moreover, for 8 dp (all energies), many events are only 'accidentally' assigned to their correct multiplicity. In order to reduce these uncertainties, the number of dp in NeuLAND should be increased and the physics list uncertainties should be reduced. To do the latter, both accurate benchmark results and physics-list model improvements are needed, especially in the energy region around 200 MeV.

C: Experimental Verification

The performance of the new DNN algorithm was further explored by experimental verification. For this procedure, the same simulation geometry and experimental data was used as for the physics-list benchmarking in Ref. [13]. This situation corresponds to the NeuLAND commissioning run [20] at the SAMURAI setup [21] at RIBF, RIKEN, Japan. For this commissioning run, proton beams of 252.7 MeV and 109.1 MeV (different runs) were shot on a fixed ^{7}Li target to induce the ^{7}Li$(p,n)^7$Be charge-exchange reaction. We have tested both our new DNN algorithm as well as the old TDR algorithm by extracting the ground-state-to-ground-state cross section of this reaction. For this procedure, we only considered the neutron detection by NeuLAND and ignored the ^{7}Be ion.

Cross sections were extracted according to the procedures described in Ref. [22]. The detection efficiencies were obtained from simulation data and a specially dedicated event generator was used for this. For both proton energies, a small but measurable increase in statistics was found for the DNN algorithm with respect to the TDR algorithm. However, since NeuLAND was only 4 dp thick during this experiment (only 4 dp) and the neutron energy was so low, the NeuLAND signal clusters were not very complex. As a result, all signal selection algorithms gave roughly the same performance and only a small increase in multiplicity performance was found when using the DNN algorithm.

The resulting cross sections of the TDR and DNN algorithms were compared to the cross sections obtained with a model-independent analysis algorithm of NeuLAND. This algorithm is only usable for the present experiment and uses the a-priori known fact that all events are 1-neutron events, meaning that for each event a single showerhead can be found by simply selecting the minimal Time-Of-Flight (TOF) signal. We will refer to this algorithm as 'MinTOF' from now on. The resulting cross sections are shown in Fig. 13. The unit of the differential cross section is [events/sr] since the integrated beam charge was not measured during this experiment.
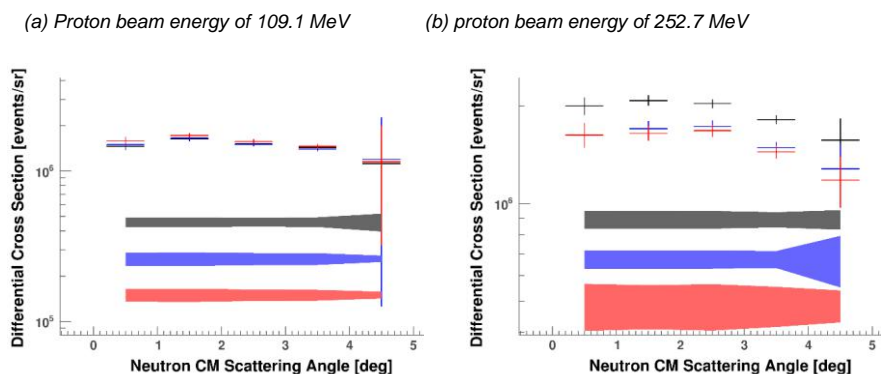
(a) Proton beam energy of 109.1 MeV   (b) proton beam energy of 252.7 MeV

Fig. 13: Cross sections of the ground-state-to-ground-state transition in $^7Li(p,n)^7Be$ for different proton energies. The cross sections were extracted from the neutron detection with NeuLAND, ignoring the ^7Be. Various NeuLAND analysis algorithms were employed. The red graphs show the result of the DNN algorithm, the blue graphs show the result of the old TDR algorithm and the black graphs show the result of the perfect MinTOF algorithm. See text for further details.

From Fig. 13 it is clear that for 109.1 MeV, all analysis algorithms yield the same cross section once the corresponding efficiency correction is applied, since cross section is basically counts/(efficiency*acceptance). However, at 252.7 MeV both the TDR and the DNN algorithm underestimate the cross section by about 20 %, which cannot be sufficiently explained by our a-priori estimated physics-list uncertainties. However, an a-posteriori analysis using the MinTOF-analysed data revealed that the 20% underestimation is nevertheless caused by the mismatch between physics list and reality. This further supports our claim that a better understanding of the physics list is needed in order to use our DNN algorithm.

CONCLUSION

We conclude that our new DNN algorithm provides us with a better efficiency than the old TDR method for showerhead identification, which was the reason for developing the new algorithm. A higher number of counts was found for all studied NeuLAND configurations (8 dp, 16 dp and 30 dp) and for all neutron energies (200 MeV, 600 MeV and 1000 MeV). This was also the case for the experimental data of the NeuLAND commissioning run (4 dp and 252.7 MeV, 109.1 MeV). However, systematic uncertainties (which the previous TDR method also suffers from) inhibit our use of the new algorithm. The systematic uncertainties are mainly caused by our lack of understanding of the physics list and are particularly large in the energy range 200 MeV – 250 MeV. However, for a NeuLAND configuration of 8 dp, uncertainties are also large at higher neutron energies and the multiplicity determination also contains significant uncertainties. For this reason, we recommend increasing the number of NeuLAND double-planes as soon as possible (16 will suffice, but possibly a lower number could suffice too) and to improve our understanding of the physics lists used in the simulations. The latter should be done both by providing accurate benchmarks and by improving the physics-list model.

Bibliography

[1] Al-Turany, M., Bertini, D., Karabowicz, R., Kresan, D., Malzacher, P., Stockmanns, T., Uhlig, F. (2012). *The FairRoot framework.* Journal of Physics Conference Series. 396. 2001-. 10.1088/1742-6596/396/2/022001. See https://fairroot.gsi.de/

[2] Available at https://github.com/ENSARRootGroup/EnsarRoot

[3] Cabanelas, P., Alvarez-Pol, H., Galiana, E., González-Rozas, Y. (2018). *ENSARRoot: The framework for simulation and data analysis for ENSAR.* Journal of Physics: Conference Series. 1024. 012038. 10.1088/1742-6596/1024/1/012038.

[4] J.A. Garzón, P. Cabanelas, Nucl. Inst. Meth. Res. A, 661 (2012) S210-S213

[5] See a description of the project in: https://www.hidronav.es/page4.html

[6] Alvarez-Pol, H. et al. (2015). *TRAGALDABAS: A new high resolution detector for the regular study of cosmic rays.* Journal of Physics: Conference Series. 632. 012010. 10.1088/1742-6596/632/1/012010

[7] Y. Fontenla et al., PoS (ICRC2019) 072

[8] C. Hagmann, D. Lange, D. Wright, *Cosmic-ray shower generator (CRY) for Monte Carlo transport codes.* 2007 IEEE Nuclear Science Symposium Conference Record, Honolulu, HI, 2007, pp. 1143-1146.

[9] The R3B collaboration, "Technical Report for the Design, Construction and Commissioning of NeuLAND: The High-Resolution Neutron Time-of-Flight Spectrometer for R3B," *GSI and Collaborators* (2011).

[10] The R3B collaboration, "Technical Proposal for the Design, Construction, Commissioning and Operation of R3B: A universal setup for kinematical complete measurements of Reactions with Relativistic Radioactive Beams," *GSI Helmholtzzentrum für Schwerionenforschung* (2005).

[11] FAIR, "Baseline Technical Report," *GSI*, vol. 2 (2006).

[12] C. A. Douma *et al.*, "Feasibility study for the use of a VETO wall for the NeuLAND neutron detector," *Nucl. Instr. Meth. Phys. Res. A*, **930** 203-209 (2019).

[13] J. Mayer, "Charting NeuLAND: Towards multi-neutron reconstruction with the New Large Area Neutron Detector and The virtual γ-ray spectrometer G4Horus" *PhD thesis, Universität zu Köln, Germany* (2018).

[14] Y. LeCun *et al.*, "Deep Learning," *Nature*, **521** 436-444 (2015).

[15] D. Guest *et al.*, "Deep Learning and Its Application to LHC Physics," *Ann. Rev. Nucl. Part. Science*, **68** 161-181 (2018).

[16] C. A. Douma, "Measurement of the Gamow-Teller states in ^{116}Sb and ^{122}Sb", *PhD thesis, University of Groningen, The Netherlands* (2019).

[17] E. B. Hoemann, "Neural Network analysis for NeuLAND & Radiation exposure at interventional radiology," *MSc. thesis, University of Cologne, Germany* (2019).

[18] C. A. Douma, "DNN module for R3BRoot," https://github.com/ChristiaanAlwin/NeuLAND_DNN.git

Commenté [LYD1]: ¿???

[19] The SAMURAI collaboration, "Investigation of the 4n system at SAMURAI by measuring p,pa quasi-free scattering at large momentum transfer in complete kinematics," *Proposal for a Nuclear-Physics Experiment at the RI Beam Factory* (2014).

[20] K. Boretzky *et al.*, "NeuLAND - from double-planes to the demonstrator," *GSI Report,* vol. 1, MU-NUSTAR-NR-12 (2015).

[21] H. Otsu *et al.*, "SAMURAI in its operating phase for RIBF users," *Nucl. Instr. Meth. Phys. Res. B*, **376** 175-179 (2016).

[22] C. A. Douma *et al.*, "Gamow-Teller strength distributions of ^{116}Sb and ^{122}Sb using the (^{3}He,t) charge-exchange reaction," *Eur. Phys. J. A*, **56** 2 51 (2020).

Section authors and collaborators:

Section 2: Tracking algorithms implementations

P. Cabanelas[1], J. Cuenca[1], H. Alvarez-Pol[1], Y. Fontenla[1], J.A. Garzón Heydt[1]

[1]IGFAE, Univ. Santiago de Compostela, Santiago de Compostela, Spain

Section 3: Implementation of benchmarks and experimental setups.

E. Galiana[1,2], P. Teubig[2], D. Galaviz[2], P. Cabanelas[1], H. Alvarez-Pol[1],

[1]IGFAE, Univ. Santiago de Compostela, Santiago de Compostela, Spain

[2]Faculdade de Ciências da Universidade de Lisboa, Lisboa, Portugal

Section 4: Development of a Deep Neural Network for the Data Analysis of the NeuLAND Neutron Detector

C. A. Douma[1], E. B. Hoemann[2], J. Kahlbow[3], N. Kalantar-Nayestanaki[1] and J. Mayer[4]

[1]KVI-CART, University of Groningen, Groningen, The Netherlands

[2]Institute for Nuclear Physics, University of Cologne, Cologne, Germany

[3]Technische Universität Darmstadt, Darmstadt, Germany

[4]Institut für Kernphysik, Universität zu Köln, Köln, Germany